Received: 17 April 2018 | Revised: 11 June 2018 | Accepted: 19 June 2018

DOI: 10.1002/cne.24500

WILEY JCN RESEARCH IN SYSTEMS NEUROSCIENCE THE JOURNAL OF COMPARATIVE NEUROLOGY

RESEARCH ARTICLE

Target-specific forebrain projections and appropriate synaptic inputs of hESC-derived dopamine neurons grafted to the midbrain of parkinsonian rats

Tiago Cardoso[1,2] | Andrew F. Adler[1,2] | Bengt Mattsson[1,2] | Deirdre B. Hoban[1,2] | Sara Nolbrant[1,2] | Jenny Nelander Wahlestedt[1,2] | Agnete Kirkeby[1,3] | Shane Grealish[1,2] | Anders Björklund[1] | Malin Parmar[1,2]

[1]Developmental and Regenerative Neurobiology, Department of Experimental Medical Science, Lund University, Lund, Sweden

[2]Lund Stem Cell Center, Lund University, Lund, Sweden

[3]Danish Stem Cell Center (DanStem), University of Copenhagen, Copenhagen, Denmark

Correspondence
Malin Parmar, Department of Experimental Medical Science, Lund Stem Cell Center, Lund University, Lund 22184, Sweden.
Email: malin.parmar@med.lu.se

Funding information
Hjärnfonden; Parkinsonfonden; Seventh Framework Programme, Grant/Award Number: ERC Grant Agreement no. 30971 NeuroStemcellRepair (no. 602278); Vetenskapsrådet, Grant/Award Number: 2016-0087370862601/ Bagadilico; New York Stem Cell Foundation; Strategic Research Area at Lund University Multipark

Abstract

Dopamine (DA) neurons derived from human embryonic stem cells (hESCs) are a promising unlimited source of cells for cell replacement therapy in Parkinson's disease (PD). A number of studies have demonstrated functionality of DA neurons originating from hESCs when grafted to the striatum of rodent and non-human primate models of PD. However, several questions remain in regard to their axonal outgrowth potential and capacity to integrate into host circuitry. Here, ventral midbrain (VM) patterned hESC-derived progenitors were grafted into the midbrain of 6-hydroxydopamine-lesioned rats, and analyzed at 6, 18, and 24 weeks for a time-course evaluation of specificity and extent of graft-derived fiber outgrowth as well as potential for functional recovery. To investigate synaptic integration of the transplanted cells, we used rabies-based monosynaptic tracing to reveal the origin and extent of host presynaptic inputs to grafts at 6 weeks. The results reveal the capacity of grafted neurons to extend axonal projections toward appropriate forebrain target structures progressively over 24 weeks. The timing and extent of graft-derived dopaminergic fibers innervating the dorsolateral striatum matched reduction in amphetamine-induced rotational asymmetry in the animals where recovery could be observed. Monosynaptic tracing demonstrated that grafted cells integrate with host circuitry 6 weeks after transplantation, in a manner that is comparable with endogenous midbrain connectivity. Thus, we demonstrate that VM patterned hESC-derived progenitors grafted to midbrain have the capacity to extensively innervate appropriate forebrain targets, integrate into the host circuitry and that functional recovery can be achieved when grafting fetal or hESC-derived DA neurons to the midbrain.

KEYWORDS

cell transplantation, dopaminergic neurons, human embryonic stem cells, Parkinson's disease, rabies-based tracing, RRID: AB_10807945, RRID: AB_11034569, RRID: AB_1141717, RRID: AB_177511, RRID: AB_2333092, RRID: AB_300798, RRID: AB_390204, RRID: AB_572263, RRID: AB_627128

1 | INTRODUCTION

Stem cell therapy for Parkinson's disease (PD) is rapidly moving towards clinical trial (Barker, Parmar, Studer, & Takahashi, 2017). Several recently published studies have demonstrated maturation and function of dopamine (DA) neurons derived from human pluripotent stem cells (hPSCs) after transplantation (Chen et al., 2016; Grealish et al., 2014; Kikuchi et al., 2017; Kirkeby et al., 2012; Kriks et al., 2011; Steinbeck et al., 2015). With few exceptions, these studies have been conducted after ectopic, intrastriatal graft placement in rodents

and primates—mimicking the graft placement in clinical trials conducted with fetal ventral midbrain (VM) tissue (Barker, Drouin-Ouellet, & Parmar, 2015). These studies clearly demonstrate the ability of stem cell-derived DA neurons to release DA and restore motor functions in animal models of PD with an efficacy and timing comparable to primary human fetal cells.

An important predictor of successful graft function in patients is the ability of the grafted DA neurons to reinnervate the denervated striatum in the host brain (Li et al., 2016). A critical step in developing effective stem cell-based transplantation therapies is to better understand the innervation capacity of the transplanted cells, as well as the extent of afferent inputs from the host, with the aim of re-establishing connectivity that is similar to healthy endogenous circuitry. The ability of hPSC-derived neurons to extend axons across large distances sufficient to reinnervate the human brain has been modeled experimentally using intrastriatal transplantation in non-human primates (Kikuchi et al., 2017; Morizane et al., 2017; Wakeman et al., 2017). Transplantation of VM patterned progenitors into the ventral midbrain of rat models of PD–that is, the site where these cells normally reside–offers an interesting alternative model to explore outgrowth capacity and specificity in greater detail. We have previously shown that intranigral grafts of human embryonic stem cell (hESC)-derived VM progenitors, like their fetal counterparts, can extend axons over long distances to reinnervate distant forebrain targets (Grealish et al., 2014; Wictorin, Brundin, Sauer, Lindvall, & Bjorklund, 1992).

In this study, we further develop this approach to transplant VM patterned hESC-derived neural progenitors to the midbrain of a rat model of PD to assess temporal aspects of long-distance fiber outgrowth and graft integration. Using three-dimensional (3D) brain reconstruction of the distribution of graft-derived fibers, we assessed target-specific innervation along the nigrostriatal pathway (NSP) and the medial forebrain bundle (MFB) toward target forebrain structures. These target structures include the dorsal striatum (the prime target of A9 nigral neurons), as well as targets of the A10 neurons of the ventral tegmental area (VTA), that is, nucleus accumbens (NAc), septum and medial prefrontal cortex (PFC). Rabies-based monosynaptic tracing has already provided a more comprehensive identification of normal inputs to DA neurons in the VTA and substantia nigra (SN) in the intact brain (Beier et al., 2015; Faget et al., 2016; Lerner et al., 2015; Menegas et al., 2015; Watabe-Uchida, Zhu, Ogawa, Vamanrao, & Uchida, 2012), and we now use this technique to map the origins and extent of synaptic inputs to graft-derived neurons and determine how hESC-derived neurons integrate into the host brain when grafted into their normal anatomical location, the midbrain.

The results demonstrate that while the transplanted neurons progressively innervate their normal target structures over 6 months, they have been contacted by appropriate presynaptic host neurons already by 6 weeks after grafting. Analysis of behavioral recovery suggests that the timing of graft-mediated functional recovery after intranigral grafting corresponds to the time of arrival of graft-derived axonal innervation in the correct target structures, rather than that of the establishment of presynaptic partners from the host, which also matches the timing of behavioral recovery reported in other studies where the cells are transplanted to the striatum (Brundin et al., 1986; Lelos et al., 2016).

2 | METHODS

2.1 | Research animals

Adult (<180 g) female, athymic "nude" rats were purchased from Harlan Laboratories (Hsd:RH-*Foxn1*^{rnu}) and housed in individual ventilated cages with ad libitum access to food and water, under a 12-hr light/dark cycle. Adult (<1 year) male, athymic "nude" rats (Crl:NIH-*Foxn1*^{rnu}) were purchased from Charles River as hosts for the human fetal midbrain tissue. Female adult (225–250 g) Sprague–Dawley rats were purchased from Charles River and housed as described above but in standard caging. All procedures were conducted in accordance with the European Union Directive (2010/63/EU), follow 3R principles, and were approved by the local ethical committee for the use of laboratory animals and the Swedish Department of Agriculture (Jordbruksverket).

2.2 | Experimental overview

All rats received a unilateral injection of 6-hydroxydopamine to the MFB, and the efficacy of lesion was confirmed by amphetamine-induced rotations 4 weeks later.

Sprague–Dawley rats were used as recipients for transplantation experiments lasting 18 weeks or less. These animals were immunosuppressed with daily injections of cyclosporine (10 mg/kg/day, intraperitoneally; Apoteksbolaget, Sweden), starting 2 days prior to transplantation until the end of the experiment to prevent graft rejection. Athymic nude rats were used as recipients for transplantation experiments lasting >18 weeks.

2.2.1 | Temporal profiling of graft-derived fiber outgrowth

For temporal assessment of graft-derived fiber outgrowth, all animals (n = 30) received a transplant of hESC-derived neurons into the midbrain and were allocated to three different groups pertaining to three different graft survival time points: 6 weeks (n = 10), 18 weeks (n = 10), and 24 weeks (n = 10).

Animals that died before the experimental endpoint were removed from further analysis. Following perfusion and histological analysis, only the animals with surviving grafts that were discretely placed within the midbrain were included in the final analysis: 6 weeks (n = 6), 18 weeks (n = 6), and 24 weeks (n = 5).

2.2.2 | Endogenous connectivity and host-to-graft tracing experiments

To study endogenous connectivity in the midbrain, un-lesioned age- and sex-matched Sprague–Dawley rats (n = 5) were injected in the midbrain with lentivirus expressing the rabies helper construct. Four weeks later, these animals received ΔG-rabies injection at the same site and were perfused 7 days later. To assess host-to-graft connectivity at 6 weeks, animals (n = 10) were transplanted with hESC-derived neurons expressing the rabies helper construct into the midbrain. ΔG-rabies was injected at the site of transplantation after 5 weeks and the animals were perfused 7 days later for histological analysis.

2.3 | ΔG-rabies and lentivirus production

EnvA-pseudotyped ΔG-rabies was produced as described in Grealish et al. (2015). Titers were 20–30 × 10^6 TU/ml and a working dilution of 5% was used for injection in vivo. The construct for the tracing vector was purchased from Addgene (ID: 30195). High-titer preparations of lentiviral particles were produced as previously described (Zufferey, Nagy, Mandel, Naldini, & Trono, 1997). Titers were 3–9 × 10^8 U/ml and a dilution of 20% was used for in vivo experiments.

2.4 | Differentiation of hESCs and transgene expression

Human ESCs H9 (WA09, passage 31–45) and RC-17 (Roslin, passage 28) were patterned toward a ventral midbrain fate as described previously (Nolbrant, Heuer, Parmar, & Kirkeby, 2017) and used for assessing graft outcome. For the tracing studies, hESCs were repeatedly transduced with the tracing construct (Grealish et al., 2015), and the cells were transduced again at day 4 and 11–15 of differentiation using lentivirus vectors at a Multiplicity of infection (MOI) of 1.5.

2.5 | Human fetal tissue

Human fetal tissue was obtained from legally terminated embryos with approval of the Swedish National Board of Health and Welfare in accordance with existing guidelines including informed consent from women seeking elective abortions. The gestational age of each embryo was determined by measuring the crown-to-rump length and/or estimated by ultrasound measurements. Embryos were then staged according to weeks post-conception (p.c.). Fetal tissue was prepared and transplanted as a semi-crude suspension, as described in Rath et al. (2013). Individual embryos of 8 and 5.5 weeks p.c. were included in this study and transplanted into the midbrain of 6-OHDA lesioned athymic nude rats that were perfused after 24 weeks (n = 6). Histological analyses from these transplants were previously reported in Grealish et al. (2014).

2.6 | Amphetamine-induced rotations

Lesion-induced rotational bias was assessed by amphetamine challenge (intraperitoneal injection of 2.5 mg/kg of amphetamine; Apoteksbolaget, Sweden) and recorded over 90 min using an automated system (Omnitech Electronics). Full body turns toward the side of the lesion side were given positive values and turns to the opposite side given negative values—and data expressed as net turns per minute. Animals with a net score of five turns per minute or greater were considered to have successful lesions and were included in the behavioral analysis in Figure 4k.

2.7 | Surgical procedures

All surgical procedures were performed under general anesthesia using a solution of fentanyl and medetomdine (20:1) injected intraperitoneally (1 ml/kg; Apoteksbolaget, Sweden). Rats were rendered parkinsonian by unilateral injection of 6-hydroxydopamine into the right MFB, with a volume of 4 μl at 20.6 mM to the following coordinates relative to bregma: A/P -4; M/L -1.2; D/V (from dura) -7.5; tooth bar -4.

Four weeks after 6-OHDA lesion, host rats received a total dose of 75,000 hESCs at day 16 of differentiation into the midbrain in a volume of 2 μl, at a concentration 37,500 cells/μl, at a rate of 1 μl per minute and diffusion time of 2 min, to the following coordinates relative to bregma: A/P -5.2; M/L -2.3; D/V (from dura) -7; adjusted to flat head.

For fetal VM tissue transplantation, individual fetuses aged 5.5 or 8 weeks p.c. were dissociated in 20 μl and 1.5 μl per rat was transplanted to the following coordinates relative to bregma: A/P -4.6; M/L -2.2; D/V (from dura) -7; tooth bar -2.4.

For host-to-graft monosynaptic tracing experiments, ΔG-rabies at a dilution of 5% of the stock was injected in a volume of 2 μl, at a rate of 0.5 μl per minute and diffusion time of 2 min, into the transplantation site: A/P -5.2; M/L -2.3; D/V (from dura) -7; adjusted to flat head.

For the mapping of endogenous midbrain connectivity, the tracing lentiviral vector was injected into the midbrain in a volume of 2 μl, at the following coordinates relative to bregma: A/P -5.2; M/L -2.3; D/V (from dura) -7; adjusted to flat head. Four weeks later ΔG-rabies was injected in volume of 2 μl at the same site.

2.8 | Immunohistochemistry

Prior to perfusion, rats were given terminal anesthesia with a lethal dose of 60 mg/kg sodium pentobarbitone injected intraperitoneally (Apoteksbolaget, Sweden). The animals were transcardially perfused with physiological saline solution followed by ice-cold 4% paraformaldehyde. Brains were post-fixed for 2 h in 4% paraformaldehyde, transferred to 25% sucrose for 48 hr and sectioned at a 35 μm thickness (1:8 series) using a freezing microtome. Immunohistochemistry was performed on free floating sections that were incubated with primary antibodies overnight in 0.1 M KPBS solution containing 0.25% Triton-X and 5% serum for the species specific to the secondary antibody. Sections were incubated with secondary antibodies for 1 hr in the same solution. Secondary antibodies coupled with biotin or conjugated with a fluorophore were used for diaminobenzidine (DAB) or fluorescent detection, respectively. All stained sections were mounted on gelatin-coated microscope slides. DAB-developed sections were dehydrated in an ascending series of alcohols, cleared with xylene and coverslipped using DPX mountant. Fluorescent immunostainings were coverslipped using polyvinyl alcohol mounting medium with DABCO (PVA-DABCO, Sigma-Aldrich, St. Louis, Missouri, USA) and left to dry overnight.

A biotinylated tyramide signal amplification (TSA) protocol (Adams, 1992) was used to boost detection of fluorescently labeled human neural cell adhesion molecule (hNCAM) positive axons and μ-opioid receptor (MOR) positive cell bodies. After labeling with primary antibodies, sections were incubated in biotinylated secondary antibodies for 1 hr at room temperature, washed, and then incubated with ABC solution for 30 min. Sections were washed, then incubated with biotinyl tyramide (1:2,500 in KPBS containing 0.009% H_2O_2) for 30 min. hNCAM-stained sections were further amplified with a second round of ABC and biotinyl tyramide incubation. Sections were then fluorescently labeled by 2 hr incubation with fluorophore-conjugated streptavidin (1:500). Finally, sections were washed and mounted as described above.

2.9 | Antibody characterization

The following primary antibodies were used: mouse monoclonal anti-hNCAM (1:1,000 for DAB reactions, and 1:5,000 for TSA reactions; Santa Cruz Biotechnology, Dallas, Texas, USA Cat# sc-106, RRID: AB_627128), immunogen raised against CD56 positive cells of human origin and recognizes band corresponding to hNCAM in western blot of transfected 293T whole cell lysates (manufacturer information); rabbit polyclonal anti-TH (1:1,000; Millipore, Burlington, Massachusetts, USA Cat# AB152, RRID: AB_390204), raised against denatured tyrosine hydroxylase from rat pheochromocytoma, selectively labels a single band at ~62 kDa in western blot of PC12 lysates (manufacturer information); rabbit polyclonal anti-NeuN (1:1,000; Millipore, Burlington, Massachusetts, USA Cat# ABN78, RRID: AB_10807945), raised against Glutathione S-transferase-tagged recombinant mouse NeuN N-terminal fragment, specificity evaluated by western blotting in mouse brain nuclear extract (manufacturer information); mouse monoclonal anti-red fluorescent protein (RFP) (1:1,000; Abcam, Cambridge, UK Cat# ab65856, RRID: AB_1141717), raised against recombinant RFP protein expressed in *Escherichia coli*, positive control: recombinant RFP protein (manufacturer information); goat polyclonal anti-mCherry (1:1,000; SICGEN Cantanhede, Portugal Cat# AB0040-200, RRID: AB_2333092), raised against purified recombinant peptide produced in *E. coli*, detects 29 kDa band in western blot of 293HEK cell transfected with cds plasmid (manufacturer information); chicken anti-green fluorescent protein (GFP) (1:1,000; Abcam, Cambridge, UK Cat# ab13970, RRID: AB_300798), raised against recombinant full length protein corresponding to GFP, positive control: ICC/IF of GFP-transfected NIH3T3 cells (manufacturer information); guinea pig polyclonal anti-MOR (1:1,000; Millipore, Burlington, Massachusetts, USA Cat# ab5509, RRID: AB_177511), recognizes C-terminus of rat MOR corresponding to residues 384–398 (manufacturer information); rabbit polyclonal anti-Barhl1 (1:500; NovusBio, Littleton, Colorado, USA Cat# NBP1-86513, RRID: AB_11034569), developed against recombinant Barhl1 protein, specificity verified on a protein array containing target protein plus 383 other nonspecific proteins (manufacturer information); rabbit polyclonal anti-5-HT (1:10,000; ImmunoStar, Hudson, Wisconsin, USA Cat# 20080; RRID: AB_572263), raised against serotonin coupled to BSA with paraformaldehyde, the antiserum demonstrated significant labeling of rat hypothalamus, raphe nuclei, and spinal cord using indirect immunofluorescent and biotin/avidin-horseradish peroxidase techniques (manufacturer information).

2.10 | Microscopy and quantifications

All brightfield images were captured using a Leica DMI6000B microscope, while fluorescent images were acquired using a TCS SP8 laser scanning confocal microscope. For hNCAM fiber density quantifications, an ImageJ (FIJI) macro was used to automatically apply a Gaussian blur, set a local intensity threshold of a defined radius around each pixel, and quantify the pixels within the threshold and regions of interest defined with the aid of an atlas of the rat brain.

To assess the number of graft-derived dopaminergic fibers innervating the dorsolateral striatum, one section per animal depicting the same anatomical area (corresponding to +0.72 A/P relative to bregma from the Paxinos and Watson atlas of the rat brain) was immunostained with hNCAM (amplified with two rounds of TSA) and tyrosine hydroxylase (TH). Identical anatomical regions were imaged at 20× using the confocal microscope, and double positive ($hNCAM^+/TH^+$) fibers per field were manually quantified in a blinded fashion.

2.11 | 3D brain reconstruction

The 3D template of the rat brain used in this study for mapping of fiber outgrowth and ΔG-rabies traced neurons was built using a 3D software (Cinema 4D), with structural proportions based on the Paxinos and Watson rat brain atlas (Paxinos & Watson, 2005). For representation of graft-derived fiber outgrowth an entire 1:8 series of hNCAM DAB stained sections were imaged and placed in the appropriate anatomical plane in the 3D brain template. The area covered by $hNCAM^+$ outgrowth was then mapped onto each anatomical plane with outgrowth in between sections being extrapolated. Quantifications of graft volume and fiber outgrowth were performed based on this 3D map using the same Cinema 4D software. For the representation of host synaptic inputs to the graft, 1:8 series of mCherry DAB stained sections were used, with each dot representing the location of an $mCherry^+$ neuron.

2.12 | Statistical analysis

All data are presented as mean ± *SEM*. Statistical analysis was performed with GraphPad Prism 6. Statistical tests and biological replicates, representing individual animals are stated in the figures legends or results. A significance level of $\alpha = 0.05$ was set for all comparisons.

In Figure 4j, Kruskal–Wallis test was performed followed by Dunn's multiple comparisons test to compare double $hNCAM^+/TH^+$ fibers at 6, 18, and 24 weeks. In Figure 4k, paired Student *t*-test was used to assess graft-mediated recovery in amphetamine-induced rotation asymmetry, 24 weeks after transplantation with fetal tissue.

3 | RESULTS

3.1 | hESC-derived neurons grafted to the midbrain progressively extend axons to innervate appropriate forebrain targets over the course of six months

To study the dynamics of graft-derived axonal outgrowth, hESCs were patterned toward a VM fate in vitro as previously described (Nolbrant et al., 2017) and transplanted into the midbrain of 6-OHDA lesioned adult immunosuppressed or athymic (nude) rats. After 6, 18, or 24 weeks of graft maturation, the animals were sacrificed for histological analysis (Figure 1a). The results show that transplanted VM patterned neural progenitors can generate grafts rich in TH^+ neurons that survive long term after implantation into the midbrain (Figure 1b–b_2), and that the graft core does not increase in volume between 6 and 24 weeks (Figure 1c). For analysis of graft survival, size, and pattern of fiber outgrowth, we performed a 3D virtual reconstruction of the host brain using histological sections immunostained with antibodies specific for hNCAM, that labels both human neuronal cell bodies and fibers (Figure 1d–d_2).

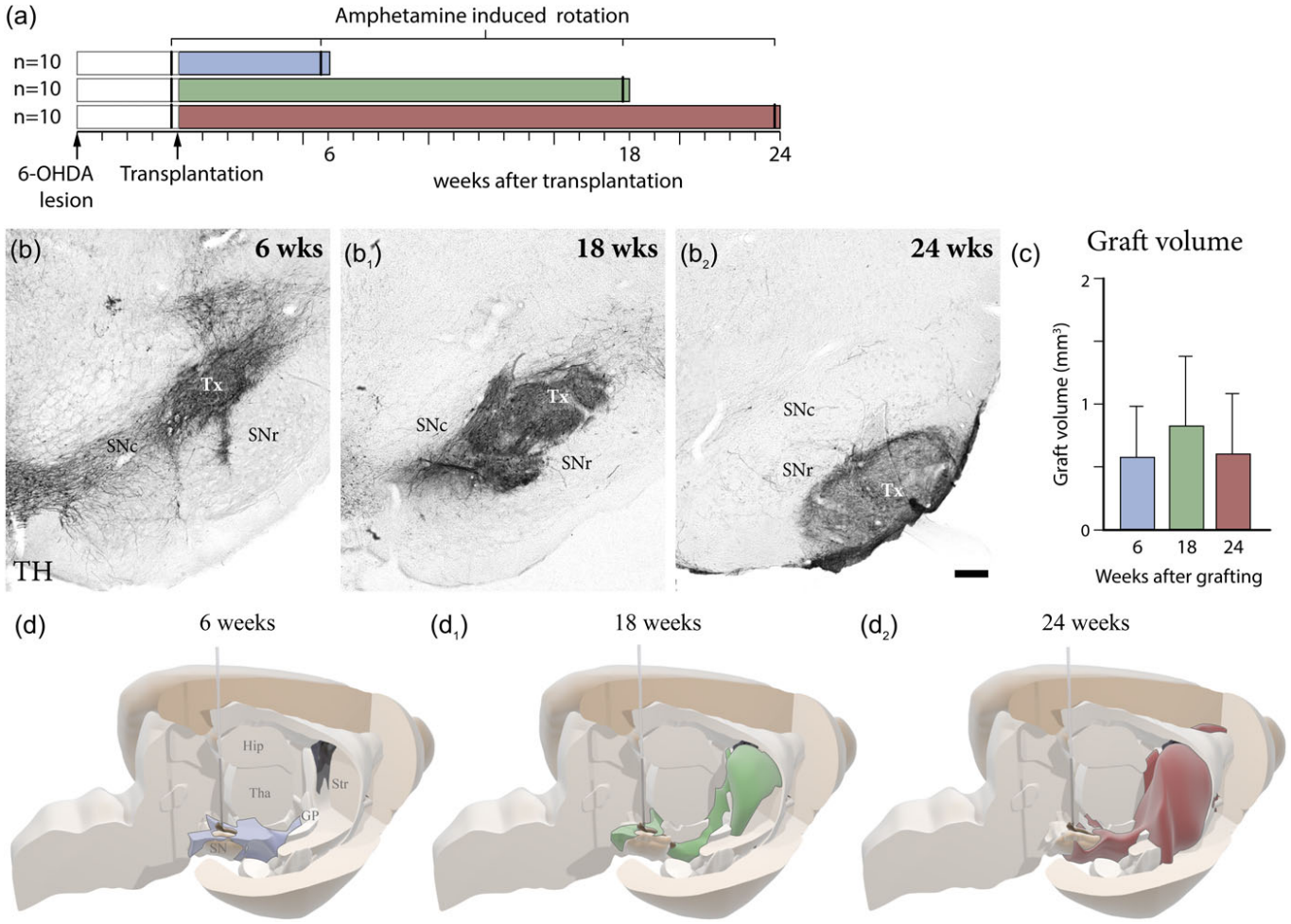

FIGURE 1 Temporal assessment of intranigral graft survival, differentiation, and axonal outgrowth. (a) Schematic overview of experimental time-plan of the three experimental groups assessing fiber outgrowth at 6, 18, and 24 weeks post-transplantation in a 6-OHDA lesioned rat model. Location and size of the transplant was confirmed using immunohistochemistry for tyrosine hydroxylase (TH) at 6 weeks (b), 18 weeks (b_1), and 24 weeks (b_2). (c) Quantification of graft volume reveals no significant change in volume from 6 weeks (n = 6), 18 weeks (n = 6), and 24 weeks (n = 5). (d) 3D representation of graft fiber outgrowth, based on the extent of hNCAM immunohistochemistry at 6 weeks (d), 18 weeks (d_1), and 24 weeks (d_2). The needle represents the site of intranigral transplantation. Scale bars: (b, b_1, b_2) = 200 μm. Hip = hippocampus; SNc = substantia nigra pars compacta; SNr = substantia nigra pars reticulata; Str = striatum; TH = tyrosine hydroxylase; Tha = thalamus; Tx = transplant [Color figure can be viewed at wileyonlinelibrary.com]

Using the 3D reconstructed images, we estimated the area covered by hNCAM$^+$ fibers at 12 evenly spaced levels along the antero-posterior (A-P) axis (Figure 2a), comparing the different groups to assess the temporal effects of fiber outgrowth along the MFB and the NSP, as well as the progressive innervation of distant A9- and A10-related forebrain target structures over the course of 24 weeks (Figure 2b,c).

At 6 weeks, the majority of hNCAM$^+$ fibers had entered the MFB and NSP, reaching the posterior hypothalamus (Figures 1d and 2b,c—corresponding to levels 4 and 5 in Figure 2a,c). At this timepoint, scarce axonal fibers were detected in the caudal striatum (corresponding to levels 6 and 7 in Figure 2a,c). Counterstaining of striatal gray matter for NeuN revealed that hNCAM$^+$ fibers were almost exclusively confined to areas devoid of neuronal cell bodies (NeuN$^-$) (white arrow in Figure 2d). Indicating that the earliest graft-derived axons to reach the striatum extended rostrally along white matter tracts. Analysis of more rostral structures, including dorsolateral striatum, NAc, and PFC, demonstrated an absence of significant graft-derived innervation of more distant target structures (Figure 3a–d).

By 18 weeks, prominent hNCAM$^+$ projections were seen to extend along the entire caudo-rostral extent of the MFB, into NAc, ventral striatum and septum—with some fibers reaching as far rostral as the medial PFC and the olfactory bulb (Figure $1d_1$ and corresponding to levels 7–11 in Figure 2a,c). At this stage dense hNCAM$^+$ terminal networks had developed in NAc and septum, as well as in part of the medial PFC (Figures 2b and 3e–g), but we could detect only few hNCAM$^+$ axon terminals in dorsolateral striatum (Figures 2b and 3h). Over the subsequent 6 weeks, we observed a marked expansion of the hNCAM$^+$ terminal network in the main A9 target, striatum, as well as in the A10 targets NAc, ventral striatum, and septum (Figures 2b), accompanied by an increased coverage of these structures by graft-derived fibers (Figure 3i–l). At this timepoint (24 weeks), we could observe an extensive ramification of hNCAM$^+$ fibers into striatal parenchyma (Figure 3l) that extend to striatal gray matter, as revealed by NeuN counterstaining, (white arrowhead in Figure 2e). These findings were confirmed by quantifying the density of fibers using automated image analysis in two of the principal A9 and A10 target structures, striatum and NAc (Figure 2f).

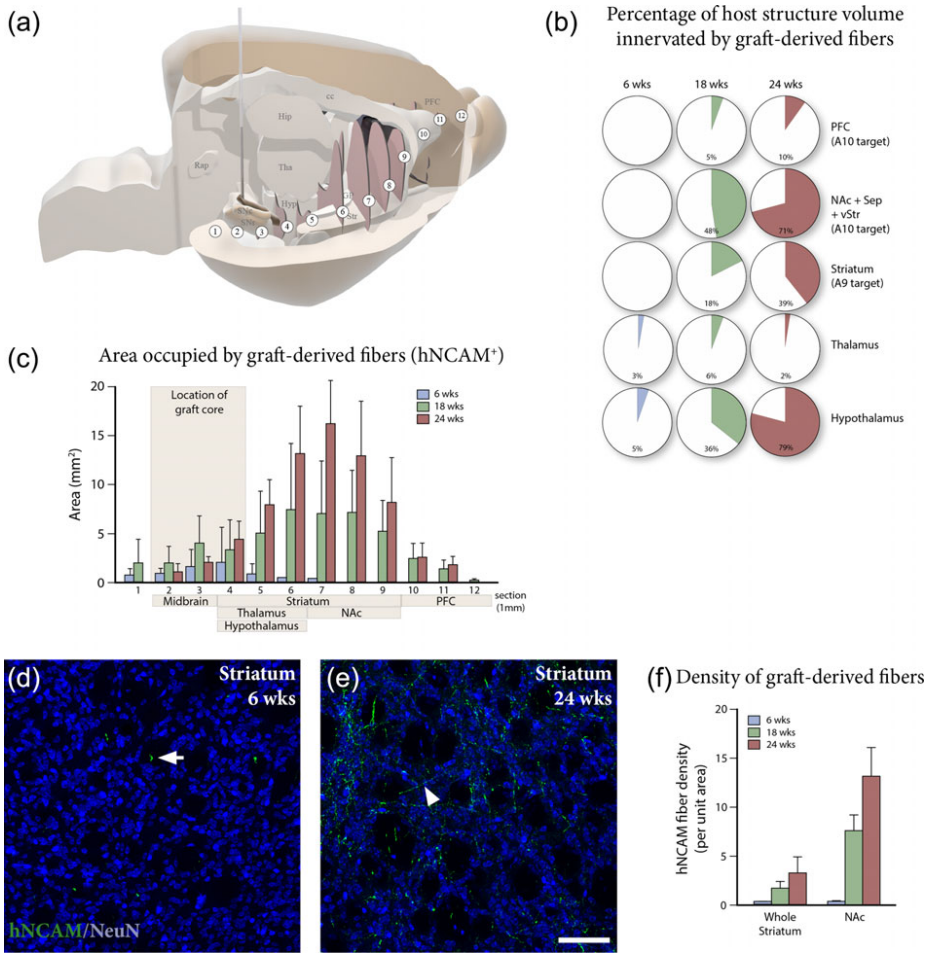

FIGURE 2 Progressive reinnervation of host forebrain target structures by graft-derived fibers. (a) 3D template of the host brain showing the position of the 12 anterior/posterior levels (white circles labeled 1–12) used to measure graft-derived axonal outgrowth at 6, 18, and 24 weeks in (c). (b) Quantification of the percentage of host target structure volume innervated by hNCAM$^+$ fibers at 6 weeks (n = 6), 18 weeks (n = 6), and 24 weeks (n = 5) post-grafting, demonstrates the progressive ramification of hNCAM$^+$ fibers over time. (c) Area innervated by hNCAM$^+$ fibers at 12 selected anterior/posterior levels (as shown in (a)) at 6 weeks (n = 6), 18 weeks (n = 6), and 24 weeks (n = 5) shows continuous outgrowth and progressive reinnervation of forebrain target structures over time. Immunostaining for hNCAM (green) and NeuN (blue) in the striatum demonstrates that graft-derived fibers are confined to white matter tracts at 6 weeks (white arrow in (d)), expanding into a fiber network in the striatal gray matter at 24 weeks (white arrowhead in (e)). (f) Quantification of hNCAM$^+$ fiber density in whole striatum and nucleus accumbens at 6 weeks (n = 6), 18 weeks (n = 6), and 24 weeks (n = 5) confirms progressive innervation of dopamine target areas over time. Scale bars: (d, e) = 100 μm. cc = corpus callosum; GP = globus pallidus; Hip = hippocampus; Hyp = hypothalamus; NAc = nucleus accumbens; PFC = prefrontal cortex; Rap = raphe nucleus; SNc = substantia nigra pars compacta; SNr = substantia nigra pars reticulata; Sep = septum; Tha = thalamus; vStr = ventral striatum [Color figure can be viewed at wileyonlinelibrary.com]

In summary, hESC-derived neurons placed in the midbrain progressively extend axons along the MFB and NSP, directed toward anatomically appropriate forebrain targets. Over the course of 24 weeks, we observed a progressively increased coverage of the forebrain areas normally innervated by midbrain DA neurons, with extensive axonal branching into the dorsal striatum (the prime target of the A9 nigral neurons), as well as into NAc, ventral striatum, septum, and medial PFC (targets of the A10 neurons in the VTA).

3.2 | Graft-derived dopaminergic innervation of dorsolateral striatum is associated with reduction in rotational bias

Specific dopaminergic (TH$^+$) innervation targeted to dorsolateral striatum is required for graft-mediated recovery of motor asymmetry in the 6-OHDA rat model (Bjorklund, Dunnett, Stenevi, Lewis, & Iversen, 1980; Dunnett, Bjorklund, Schmidt, Stenevi, & Iversen, 1983). Therefore, we proceeded to analyse the pattern of graft-derived dopaminergic outgrowth at 6 and 24 weeks after transplantation by co-staining for TH and hNCAM, monitoring the presence of double positive fibers in three structures rostral to the graft: the NSP, and the caudal and dorsolateral striatum.

Analysis of TH$^+$ fiber loss in dorsolateral striatum showed that the extent of lesion-induced forebrain DA denervation was similar at 6 (Figure 4c), 18 and 24 weeks (Figure 4f, i).

Histological analysis and quantification at 6 weeks showed sparse hNCAM$^+$/TH$^+$ fibers coursing the NSP (Figure 4a), and a few pioneering hNCAM$^+$/TH$^+$ axons were already found reaching into the caudal portion of the striatum at this stage (Figure 4b). No graft-derived TH$^+$ fibers could be detected in the dorsolateral striatum at 6 weeks (Figure 4c) and

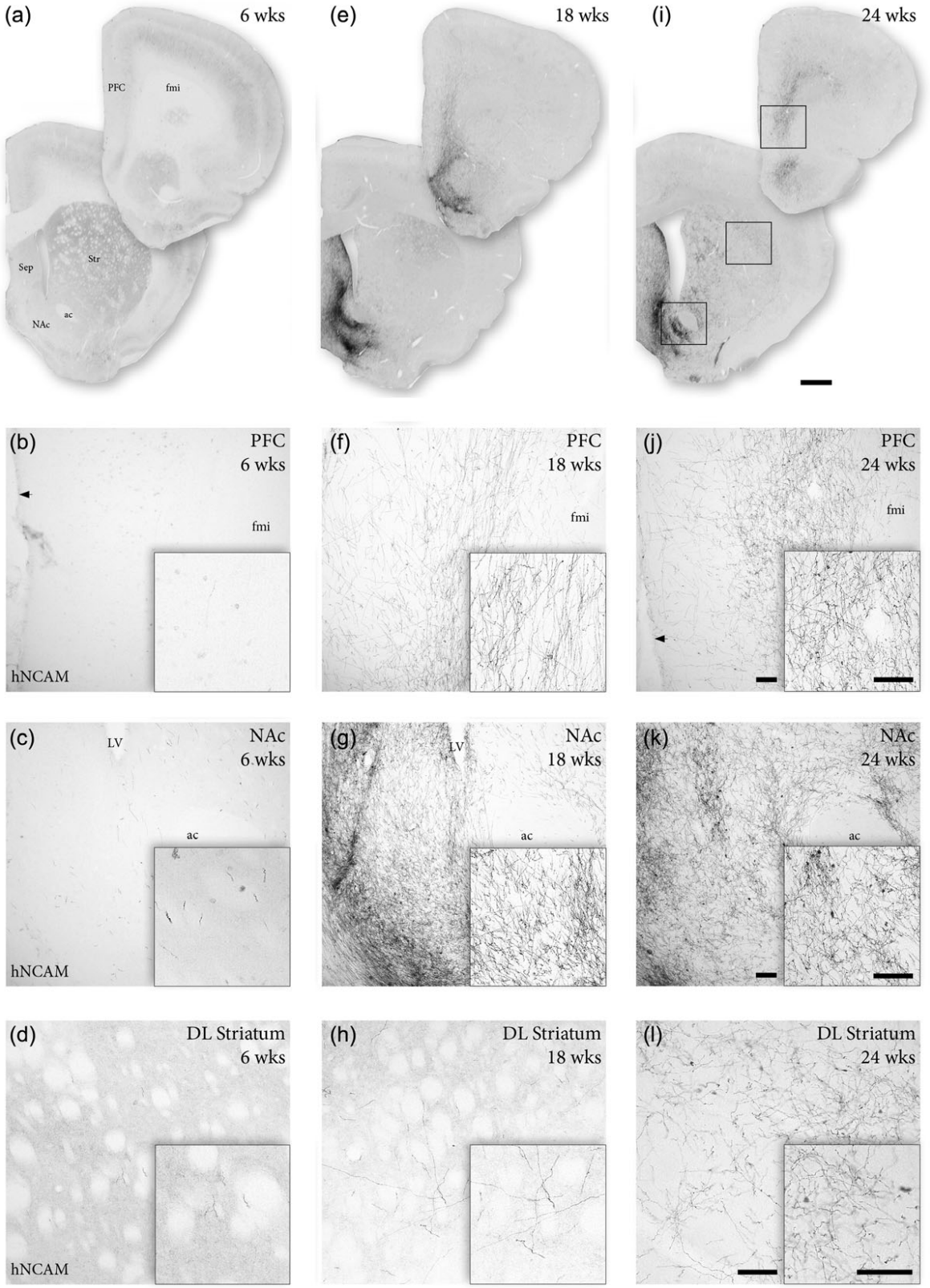

FIGURE 3 Graft-derived reinnervation of A9 and A10 target structures. (a–d) Analysis of graft-derived innervation as revealed by hNCAM immunohistochemistry 6 weeks post-transplantation, demonstrates no detectable graft fibers in PFC (b) and only few scattered axonal terminals in NAc (c) and dorsolateral striatum (d). (e–h) At 18 weeks, $hNCAM^+$ fibers were observed in the PFC (f), with extensive graft-derived innervation of the NAc (g). Individual $hNCAM^+$ fibers can be detected in dorsolateral striatum (h) at this timepoint. (i–l) At 24 weeks, abundant $hNCAM^+$ innervation was readily detectable in PFC (j) and NAc (k). At this timepoint, an extensive network of graft-derived axonal projections were observed also in dorsolateral striatum (l). Black arrow in (b) and (j) denotes the lateral ventricle. Scale bars: (a, e, i) = 1 mm. (b–d, f–h, j–l) = 100 μm. Insets in (b–d, f–h, j–l) = 100 μm. ac = anterior commissure; DL = dorsolateral; fmi = forceps minor; LV = lateral ventricle; NAc = nucleus accumbens; PFC = prefrontal cortex; Sep = septum; Str = striatum

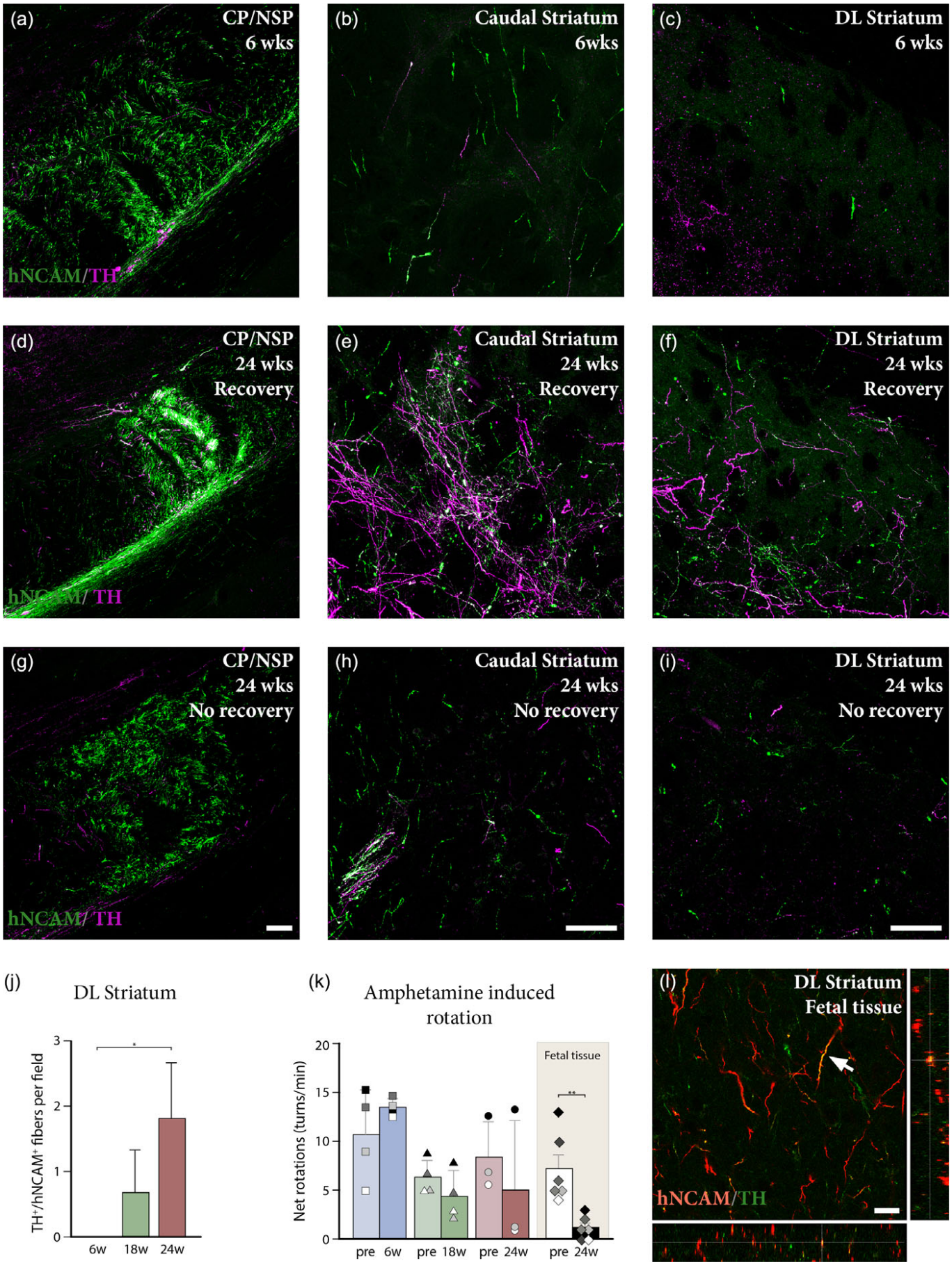
(a)
CP/NSP
6 wks
hNCAM/TH
(b)
Caudal Striatum
6wks
(c)
DL Striatum
6 wks
(d)
CP/NSP
24 wks
Recovery
(e)
Caudal Striatum
24 wks
Recovery
(f)
DL Striatum
24 wks
Recovery
(g)
CP/NSP
24 wks
No recovery
hNCAM/ TH
(h)
Caudal Striatum
24 wks
No recovery
(i)
DL Striatum
24 wks
No recovery
(j)
DL Striatum
TH+/hNCAM+ fibers per field
0
1
2
3
*
6w
18w
24w
(k)
Amphetamine induced rotation
Net rotations (turns/min)
0
5
10
15
20
Fetal tissue
**
pre 6w
pre 18w
pre 24w
pre 24w
(l)
DL Striatum
Fetal tissue
hNCAM/TH

no behavioral recovery was observed at this stage (squares, Figure 4k). At 18 weeks post-grafting, the appearance of graft-derived hNCAM$^+$/TH$^+$ axonal projections in the dorsolateral striatum (Figure 4j) coincided with a trend of reduction in the amphetamine-induced rotation scores (triangles in Figure 4k). At 24 weeks, more hNCAM$^+$/TH$^+$ fibers were present in the caudal and dorsolateral striatum (Figure 4e,f,j), and at this timepoint two out of three animals showed recovery in rotation scores (circles, Figure 4k). At this stage, double hNCAM$^+$/TH$^+$ fibers could also be detected in other dopaminergic target structures, such as NAc and cortex as previously described (Grealish et al., 2014). However, the overall distribution of hNCAM$^+$/TH$^-$ fibers was more extensive than the hNCAM$^+$/TH$^+$ fibers, reflecting the heterogenous composition of the transplants.

A closer look at individual post-transplantation rotation scores from the 24-week survival group revealed two distinct behavioral responses elicited by the amphetamine challenge. One rat (black circle in Figure 4k) showed no behavioral recovery (net score pre-transplantation = 13 turns/min; post-transplantation = 13 turns/min) and two rats (gray and white circles in Figure 4k) exhibited a pronounced rotational bias attenuation (gray circle: net score pre-transplantation = 7 turns/min, post-transplantation = 1 turns/min; white circle: net score pre-transplantation = 6 turns/min; post-transplantation = 1 turns/min). Despite the similarities between graft volume and placement, the rat that did not recover (black circle in Figure 4k) revealed more limited hNCAM$^+$/TH$^+$ outgrowth directed toward the striatum suggesting that sufficient innervation is necessary for behavioral recovery (Figure 4g–i).

This is supported by previous experiments using intrastriatal transplantation of fetal and hESC-derived cells (Kirkeby et al., 2012; Rath et al., 2013). Here, we confirmed these observations by assessing rotational recovery in animals transplanted with human fetal VM tissue. We have previously shown that fetal VM cells provide significant innervation of the A9 target structures in a more extensive manner than hESC-derived progenitors when analyzed at the same timepoint (Grealish et al., 2014). Here, we analyzed graft-mediated functional recovery data in the amphetamine-induced rotation test performed on the animals transplanted with fetal VM tissue. This revealed that grafts of human fetal VM tissue placed in the midbrain more consistently normalized amphetamine-induced rotations by 24 weeks (diamonds, Figure 4k) compared to grafts of hESC-derived progenitors (circles, Figure 4k), associated with a dense hNCAM$^+$/TH$^+$ innervation of dorsolateral striatum (Figure 4l).

In summary, this data highlights that long-distance, target-specific dopaminergic innervation to the dorsolateral striatum from human VM progenitors of hESC or fetal origin coincides temporally with graft-mediated normalization of rotational bias at 24 weeks.

3.3 | Monosynaptic tracing reveals early host-to-graft connectivity

Monosynaptic tracing allows for unambiguous identification of first-order inputs onto a defined *starter* population of neurons, by taking advantage of the selective retrograde transsynaptic spread of rabies virus (Wickersham et al., 2007). First, we used the system to create a reference map of the endogenous connectivity of the neurons located in the rat midbrain. For this purpose, a lentivirus expressing the rabies helper construct under control of the human synapsin promoter that includes histone-tagged GFP (for unambiguous identification of starter cells); TVA receptor (required for selective primary infection with EnvA-pseudotyped rabies); and rabies glycoprotein (required for transsynaptic spread of glycoprotein-deleted [Δ*G*] rabies), was injected into the midbrain of naïve Sprague–Dawley rats at the same coordinates used for transplantation. Four weeks later, EnvA-pseudotyped Δ*G*-rabies was injected at the same site to label synaptic inputs to starter neurons located in the area of the midbrain corresponding to the graft site (Figure 5a). As evident from the 3D reconstruction (Figure 5b), the input neurons labeled are in agreement with current knowledge of basal ganglia anatomy (Gerfen & Bolam, 2010) and the pattern of afferent connectivity to the dopaminergic neurons of the midbrain reported previously (Watabe-Uchida et al., 2012).

Next, we mapped the host presynaptic input to the grafted cells 6 weeks after transplantation. For that purpose, hESC-derived neurons expressing the rabies helper construct were transplanted into the midbrain. Five weeks post-transplantation EnvA-pseudotyped Δ*G*-rabies encoding mCherry was injected at the transplant site to label presynaptic inputs to the graft (Figure 5a). Hence, grafted starter neurons expressed both GFP (green) and mCherry (red), while host neurons making synaptic contact onto grafted neurons expressed mCherry only. One week after Δ*G*-rabies injection the animals were sacrificed for histological analysis.

FIGURE 4 Outgrowth of graft-derived dopaminergic fibers and related functional outcome. (a–c) Analysis of double positive hNCAM$^+$/TH$^+$ fibers at different levels in the host brain at 6 weeks post-grafting revealed the presence of some graft-derived dopaminergic fibers coursing through the cerebral peduncle/nigrostriatal pathway (a), reaching the caudal portion of the striatum (b). Despite the presence of lesion-spared endogenous dopaminergic fibers (hNCAM$^-$/TH$^+$), no double positive fibers were detected in dorsolateral striatum at this stage (c). (d–f) After 24 weeks, dopaminergic fibers of graft origin were seen coursing along the cerebral peduncle/nigrostriatal pathway in large numbers (d), providing dense innervation of the caudal striatum (e). Significant hNCAM$^+$/TH$^+$ innervation was readily detectable in dorsolateral striatum at this stage (f). (g–i) Analysis of graft-derived dopaminergic innervation in one animal in the 24-week group with no behavioral recovery showed few hNCAM$^+$/TH$^+$ fibers coursing via the cerebral peduncle/nigrostriatal pathway (g), with scattered fibers reaching the caudal striatum (h). Sparse double positive fibers can be seen reaching dorsolateral striatum (i) in this animal. (j) Quantification of hNCAM$^+$/TH$^+$ positive fibers in dorsolateral striatum at 6 weeks (n = 5), 18 weeks (n = 5), and 24 weeks (n = 6) revealed a progressive increase in the density of graft-derived dopaminergic fibers in this structure over time (Kruskal–Wallis, $\chi^2_{(2)}$ = 7.658, p < .01, Dunn's multiple comparisons test revealed a significant difference between the 6 and 24 week groups, p < .05). (k) Assessment of amphetamine-induced rotational bias pre- and post-transplantation revealed progressive graft-mediated functional recovery at 6 weeks (n = 4; squares in (k)), 18 weeks (n = 4; triangles in (k)), and 24 weeks (n = 3; circles in (k)). Animals that received grafts of human fetal midbrain tissue (n = 6; diamonds in (k)), demonstrated significant recovery (t_5 = 4.743, p < .01) at 24 weeks post-transplantation. (l) Analysis of graft-derived dopaminergic innervation of the dorsolateral striatum by fetal tissue transplants reveals several hNCAM$^+$/TH$^+$ fibers (white arrow). Scale bars: (a, d, g) = 100 μm. (b, c, e, f, h, i) = 100 μm. (l) = 20 μm. * = p < .05; ** = p < .01; CP/NSP = cerebral peduncle/nigrostriatal pathway; DL = dorsolateral [Color figure can be viewed at wileyonlinelibrary.com]

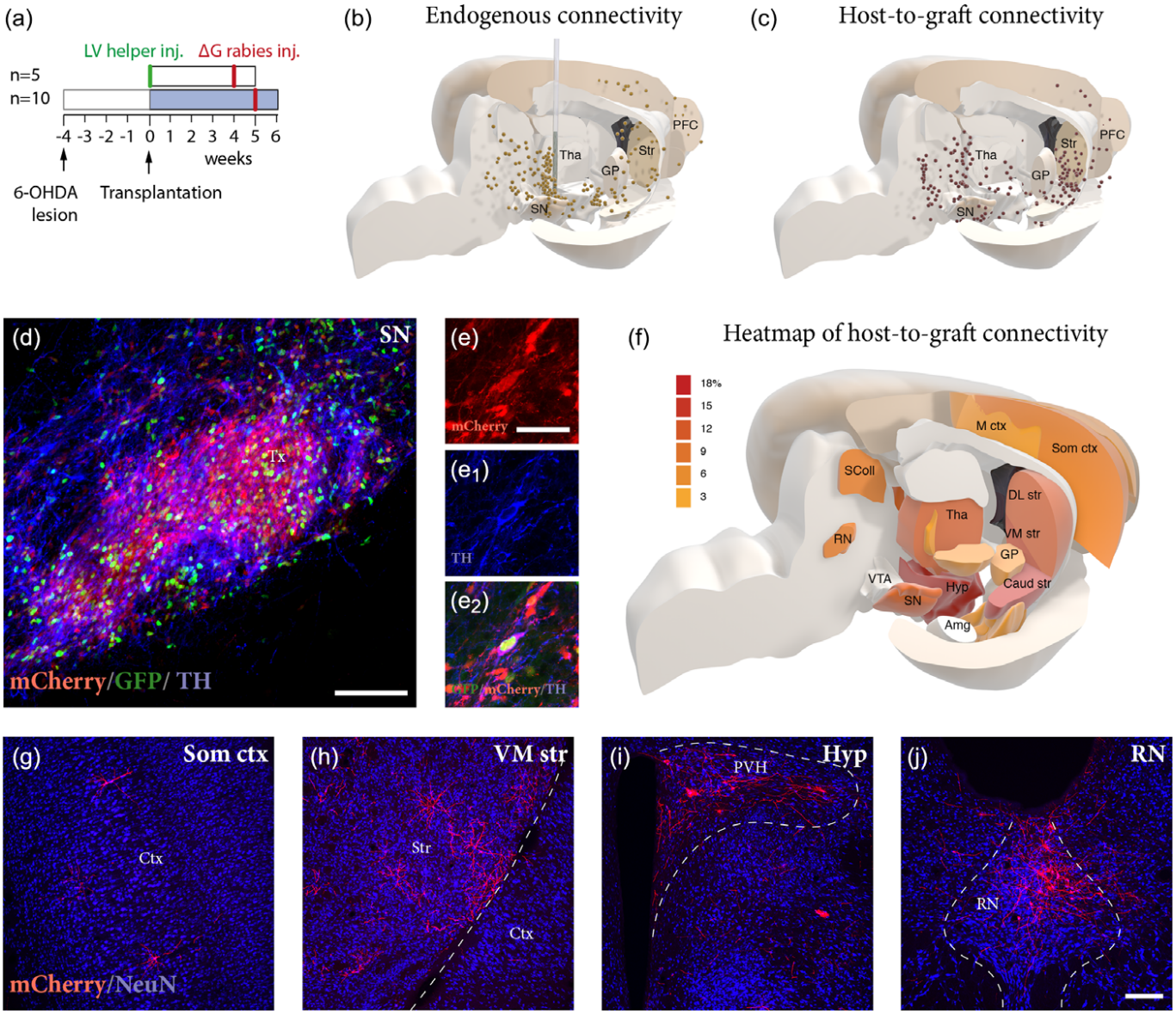

FIGURE 5 Synaptic host-to-graft integration revealed by monosynaptic tracing at 6 weeks matches endogenous connectivity. (a) Experimental design for assessment of endogenous connectivity using monosynaptic tracing. LV-helper was used to generate starter neurons in midbrain and mCherry expressing EnvA-pseudotyped Δ*G*-rabies was used as a retrograde transsynaptic tracer to map inputs to midbrain. (b) 3D representation of endogenous synaptic inputs to midbrain of normal un-lesioned rats, as revealed by rabies tracing. Each dot represents a traced neuron ($mCherry^+$) in a 1:8 series of mCherry immunostained sections from a representative animal. (c) 3D representation of whole brain monosynaptic inputs to grafted neurons at 6 weeks revealed a pattern of traced neurons similar to that obtained from the mapping of endogenous inputs to the SN seen in (b). Histological analysis of transplants after 6 weeks revealed that a large proportion of grafted neurons expressed GFP and were selectively infected by mCherry expressing rabies (d). A significant proportion of starter neurons ($GFP^+/mCherry^+$) also expressed TH (e, e_1, e_2). (f) Heat map representing the percentage of $mCherry^+$ labeling in each defined host brain area, divided by the total number of traced neurons per brain. Color grades represent different density of labeling, with associated values (3–18%) expressed in the legend. Data compiled from six individual animals (n = 6). Analysis of traced neurons ($mCherry^+$) in the host brain revealed extensive synaptic inputs to the grafted neurons originating from structures such as somatosensory cortex (g), striatum (h), hypothalamus (i), and dorsal raphe nucleus (j). Scale bars: (d) = 100 μm. (e, e_1, e_2) = 40 μm. (g–j) = 200 μm. Amg = amygdala; Caud str = caudal striatum; Ctx = cortex; DL str = dorsolateral striatum; GP = globus pallidus; Hyp = hypothalamus; M ctx = motor cortex; PFC = prefrontal cortex; PVH = paraventricular hypothalamic nucleus; RN = raphe nucleus; SColl = superior colliculus; SN = substantia nigra; Som ctx = somatosensory cortex; Str = striatum; Tha = thalamus; VM str = ventromedial striatum; VTA = ventral tegmental area [Color figure can be viewed at wileyonlinelibrary.com]

The majority of transplanted GFP^+ cells co-expressed mCherry, indicating efficient infection of starter neurons by Δ*G*-rabies (Figure 5d). At this timepoint, up to 37% of the starter neurons had matured to the stage where TH is starting to be expressed (Figure 5d–e_2). Spatial reconstruction of the precise localization of the mCherry positive neurons using a 3D model of the rat brain, based on the Paxinos and Watson atlas (Paxinos & Watson, 2005) allowed us to obtain a comprehensive overview of whole brain afferent connectivity to the transplant (Figure 5c; see Methods for more details). At 6 weeks post-transplantation, traced host neurons ($GFP^-/mCherry^+$) were

readily detected in different host structures throughout the brain, including prefrontal and sensorimotor cortices (Figure 5f,g), striatum (Figure 5f,h), hypothalamus (Figure 5f,i), subthalamic nucleus (see Figure 6b), and dorsal raphe nucleus (Figure 5f,j). The overall pattern of the ΔG-rabies labeled neurons traced from the grafted neurons was similar in distribution to that obtained from the endogenous neurons (compare Figure 5b,c), indicating early and extensive establishment of anatomically appropriate synaptic inputs to the grafted human neurons (Figure 5g–j).

The regional identity of traced neurons in selected structures showing dense labeling (Figure 5f) was confirmed by performing a counterstain with NeuN to resolve anatomical boundaries (Figure 5g–j) and by immunostaining of regional phenotypic markers, expressed by neurons normally projecting to the DA neurons in the substantia nigra (Smith et al., 2016; Watabe-Uchida et al., 2012), including MOR in striatum (Figure 6a,a_1), Barhl1 in the subthalamic nucleus (Figure 6b,b_1) and 5-HT in the dorsal raphe nucleus (Figure 6c,c_1).

In summary, the results show that the grafted neurons in the midbrain receive presynaptic inputs from the host already at 6 weeks after transplantation, and that the overall connectivity established at this early timepoint matches well the pattern of intrinsic nigral afferents, as described in the literature using this tracing method.

4 | DISCUSSION

Cell-based therapy for PD was pioneered over 25 years ago, yet it is still at the stage of small-scale clinical trials due to the limited access to standardized fetal donor tissue (Barker et al., 2015). Stem cells have long been explored as an alternative cell source, and significant developments in the last decade now allow for the generation of an unlimited number of appropriately patterned VM progenitors from pluripotent stem cells (Steinbeck & Studer, 2015). For PD, several clinical trials using VM progenitors derived from hPSCs are planned (Abbott, 2014; Barker et al., 2017), and hPSC-derived DA neurons will also serve as important tools for further development with the aim to move from cell replacement to more complete circuit reconstruction. In this study, we use hESC-derived VM progenitors transplanted to the midbrain to better understand graft function, reinnervation capacity, and anatomical integration of human DA neurons in the 6-OHDA lesion model of PD.

Intranigral transplantation has been used previously to explore the capacity of grafted dopaminergic neuroblasts to extend axons over long distances toward their appropriate targets (Grealish et al., 2014; Isacson et al., 1995; Thompson, Grealish, Kirik, & Bjorklund, 2009; Wictorin et al., 1992). Here, we used this strategy to study the capacity of hESC-derived neurons to grow axons along the NSP and

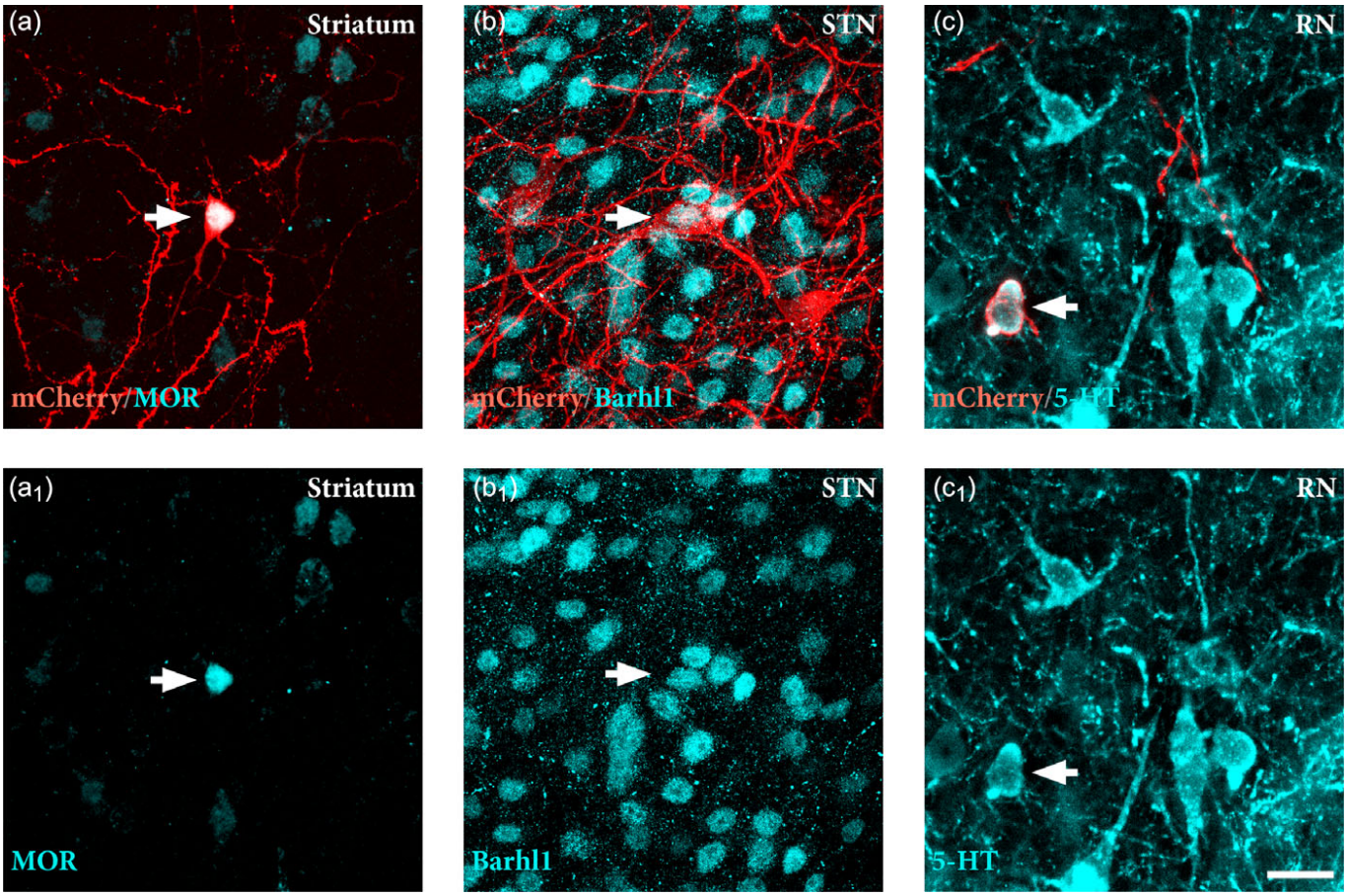

FIGURE 6 Identification of the phenotype of traced host neurons. Immunostaining for specific phenotypic markers reveals the identity of host inputs to graft. Labeled neurons in striatum co-expressed μ-opiod receptor (MOR) (a, a_1), neurons in the subthalamic nucleus (STN) co-expressed Barhl1 (b, b_1), while those in the dorsal raphe nucleus (RN) co-expressed serotonin (5-HT) (c, c_1). White arrow denotes double positive neurons for mCherry and phenotypic marker. Scale bars: (a–c_1) = 20 μm. STN = subthalamic nucleus; RN = rape nucleus; 5-HT = serotonin [Color figure can be viewed at wileyonlinelibrary.com]

MFB and progressively innervate appropriate forebrain target structures over the course of 24 weeks. At 6 weeks post-grafting, outgrowing hNCAM$^+$ fibers were seen to exit the graft in a rostral direction and extend along the MFB and NSP. At this timepoint, a few scattered axons were observed in the caudal striatum and NAc, but none were found in other target areas in the forebrain. By 18 weeks, we detected extensive innervation of A10 target structures including ventral striatum, NAc, septum, and PFC, and at 24 weeks graft-derived hNCAM$^+$ fibers had expanded further to cover a large portion of the dorsolateral striatum, the main target region for A9 DA neurons.

As with fetal tissue preparations used in clinical trials, stem cell-derived DA neurons consist of a mix of both A9 and A10 DA neuron populations, and there is currently no method to identify or separate these two populations at the progenitor stage. In agreement with this, we have previously shown that long-distance axonal outgrowth from the graft is directed toward both A9 and A10 target structures (Grealish et al., 2014). Here, we observe at 18 weeks hNCAM$^+$ fibers reaching from the graft site to the PFC and olfactory bulb over a distance of >10 mm, which is sufficient to provide full innervation of the putamen in human patients grafted with VM tissue (estimated at 5–7 mm from each graft deposit; Kordower et al., 1995). Interestingly, even though the exact graft placement varied, the fiber outgrowth pattern were similar. Thus, regardless of their dorsal/ventral location in SNc or SNr, the outgrowing fibers could be seen reaching the MFB and NSP and coursing toward appropriate forebrain target structures in a similar manner.

Our time-course analyses show that 24 weeks of graft maturation was required for the more extensive innervation of the dorsolateral striatum, that is, the functionally relevant structure for motor control in the parkinsonian rat brain. At this timepoint, we observed abundant hNCAM$^+$/TH$^+$ projections of graft origin progressing via the MFB and the NSP, providing a widespread innervation of the striatal parenchyma. At this stage, the presence of graft-derived dopaminergic fibers in the dorsolateral striatum correlated with functional recovery in some animals as assessed by amphetamine-induced rotations (Bjorklund et al., 1980; Dunnett et al., 1983; Grealish et al., 2010). When analyzing transplants of human fetal tissue grafted to the midbrain after 24 weeks, we observed efficient recovery in all animals which also correlated with hNCAM$^+$/TH$^+$ projections in the dorsolateral striatum at this point (Grealish et al., 2014). These data highlight that the long-distance hNCAM$^+$/TH$^+$ fibers observed at 24 weeks from transplants of hESC or fetal VM progenitors are capable of releasing DA to a sufficient extent to normalize rotational bias, highlighting this approach of intranigral grafting as a useful measure of reinnervation capacity now also with a functional read-out. The validity of this approach is also highlighted by one animal in the 24-week group in which the transplant failed to induce any reduction of rotational bias despite similar graft placement, size, and TH$^+$ neuron content as in the animals where the grafts had a functional effect. A closer analysis of this subject showed that the graft-derived fibers had failed to innervate the dorsolateral striatum despite the presence of abundant outgrowth toward ventral striatum and NAc (Figure 4g–i).

The time-course of functional recovery seen here—with the first signs observed at 18 weeks post-grafting and in some animals showing a complete recovery at 24 weeks—is very similar to that obtained with fetal-derived midbrain DA neurons transplanted to striatum, where the recovery in amphetamine-induced rotation emerges between 16 and 20 weeks post-grafting (Brundin et al., 1986; Lelos et al., 2016). It also matches remarkably well with the time-course of recovery in motor function (arm-hand movement and rigidity scores) seen in a patient with grafts of fetal VM tissue (Lindvall et al., 1990). Clinical observations of patients transplanted with VM tissue of fetal origin reveals that grafted neurons continue to functionally mature over the course of around 3 years (Kefalopoulou et al., 2014; Politis et al., 2010). Postmortem analysis of brain tissue from these patients suggest that fibers from grafted tissue extensively innervate the host but remain confined to appropriate target structures (Li et al., 2016). We have previously shown that the functional potency of hESC-derived DA neurons is *en par* with that of their fetal counterparts when transplanted to the striatum (Grealish et al., 2014). The current data provide further support to the equivalence of the two cell types, in terms of potency, and axonal growth capacity and dynamics, and highlight the importance of the content of DA neurons of the A9 type for graft-induced recovery of motor function in this PD model linked to efficient reinnervation of the critical striatal target—as previously demonstrated with transplants of rodent tissue (Grealish et al., 2010).

The host afferent inputs to the grafted neurons were established early, already at 6 weeks post-grafting, at a time when the outgrowing axons have yet to reach their final targets. Using monosynaptic tracing of midbrain DA neurons in the DAT-Cre mouse, it has been shown that both A9 and A10 DA neurons receive inputs from the striatum. The A9 neurons also receive relatively strong excitatory inputs from the somatosensory and motor cortices, as well as subthalamic nucleus, whereas the A10 DA neurons in the VTA receive strong inputs from the lateral hypothalamus (Watabe-Uchida et al., 2012). Using the same Δ*G*-rabies tracing method to map the afferent connectivity to the graft, we found substantial numbers of afferent neurons in the prefrontal and sensorimotor cortices, striatum, hypothalamus, subthalamic nucleus, and dorsal raphe nucleus already at 6 weeks post-transplantation. The overall distribution of the connections established by the host to the graft matches well the endogenous nigral afferent circuitry revealed by Δ*G*-rabies tracing (Watabe-Uchida et al., 2012), as well as the neuroanatomy of A9 and A10 DA neurons known from classic studies (reviewed in Gerfen & Bolam, 2010). However, despite the extent of synaptic integration observed at 6 weeks, we did not see any improvement of motor asymmetry in the amphetamine rotation test at this early timepoint, which is consistent with previous findings using fetal and hESC-derived VM progenitors (Brundin et al., 1986; Kirkeby et al., 2012; Rath et al., 2013; Wakeman et al., 2017). This finding supports the view that the primary driver of behavioral recovery in DA-dependent behavioral tests is the directed outgrowth and efficient reinnervation of appropriate forebrain targets rather than the extent of host-to-graft synaptic integration.

In conclusion, we show that intranigral grafts of VM progenitors have the capacity to extensively integrate into host circuitry and grow axonal projections toward appropriate forebrain targets over time, and that the functional recovery, as assessed by amphetamine-induced rotations, matched both the timing and extent of A9 specific graft innervation of the dorsolateral part of the striatum in the animals

where recovery could be observed. Moreover, the range of afferent inputs available to grafts placed in the midbrain, as observed here, suggests that hESC-derived DA neurons grafted to the midbrain have the capacity to go beyond simple DA neuron replacement to achieve more complete circuitry repair.

ACKNOWLEDGMENTS

The authors thank Michael Sparrenius, Sol da Rocha Baez, Ingar Nilsson, Ulla Jarl, Jenny Johansson, and Marie Persson Vejgården for excellent technical assistance, Andreas Heuer and Jessica Giacomoni for help with surgeries and tissue processing, and Jennifer Dulin and James Conner for help with TSA. The research leading to these results has received funding from the New York Stem Cell Foundation, the European Research Council under the European Union's Seventh Framework Programme: FP/2007-2013 NeuroStemcellRepair (No. 602278) and ERC Grant Agreement No. 30971, the Swedish Research Council (grant agreement 2016-00873 and 70862601/Bagadilico), Swedish Parkinson Foundation (Parkinsonfonden), Swedish Brain Foundation and the Strategic Research Area at Lund University Multipark (Multidisciplinary research in Parkinson's disease). S.G. was supported by a postdoctoral stipend from the Swedish Brain Foundation (Hjärnfonden) and M.P. is a New York Stem Cell Foundation Robertson Investigator.

ORCID

Tiago Cardoso http://orcid.org/0000-0003-2686-458X

REFERENCES

Abbott, A. (2014). Fetal-cell revival for Parkinson's. *Nature*, *510*(7504), 195–196. https://doi.org/10.1038/510195a

Adams, J. C. (1992). Biotin amplification of biotin and horseradish peroxidase signals in histochemical stains. *The Journal of Histochemistry and Cytochemistry*, *40*(10), 1457–1463. https://doi.org/10.1177/40.10.1527370

Barker, R. A., Drouin-Ouellet, J., & Parmar, M. (2015). Cell-based therapies for Parkinson disease-past insights and future potential. *Nature Reviews. Neurology*, *11*(9), 492–503. https://doi.org/10.1038/nrneurol.2015.123

Barker, R. A., Parmar, M., Studer, L., & Takahashi, J. (2017). Human trials of stem cell-derived dopamine neurons for Parkinson's disease: Dawn of a new era. *Cell Stem Cell*, *21*(5), 569–573. https://doi.org/10.1016/j.stem.2017.09.014

Beier, K. T., Steinberg, E. E., DeLoach, K. E., Xie, S., Miyamichi, K., Schwarz, L., … Luo, L. (2015). Circuit architecture of VTA dopamine neurons revealed by systematic input-output mapping. *Cell*, *162*(3), 622–634. https://doi.org/10.1016/j.cell. 2015.07.015

Bjorklund, A., Dunnett, S. B., Stenevi, U., Lewis, M. E., & Iversen, S. D. (1980). Reinnervation of the denervated striatum by substantia nigra transplants: Functional consequences as revealed by pharmacological and sensorimotor testing. *Brain Research*, *199*(2), 307–333.

Brundin, P., Nilsson, O. G., Strecker, R. E., Lindvall, O., Astedt, B., & Bjorklund, A. (1986). Behavioural effects of human fetal dopamine neurons grafted in a rat model of Parkinson's disease. *Experimental Brain Research*, *65*(1), 235–240.

Chen, Y., Xiong, M., Dong, Y., Haberman, A., Cao, J., Liu, H., … Zhang, S. C. (2016). Chemical control of grafted human PSC-derived neurons in a mouse model of Parkinson's disease. *Cell Stem Cell*, *18*(6), 817–826. https://doi.org/10.1016/j.stem.2016.03.014

Dunnett, S. B., Bjorklund, A., Schmidt, R. H., Stenevi, U., & Iversen, S. D. (1983). Intracerebral grafting of neuronal cell suspensions. IV. Behavioural recovery in rats with unilateral 6-OHDA lesions following implantation of nigral cell suspensions in different forebrain sites. *Acta Physiologica Scandinavica. Supplementum*, *522*, 29–37.

Faget, L., Osakada, F., Duan, J., Ressler, R., Johnson, A. B., Proudfoot, J. A., … Hnasko, T. S. (2016). Afferent inputs to neurotransmitter-defined cell types in the ventral tegmental area. *Cell Reports*, *15*(12), 2796–2808. https://doi.org/10.1016/j.celrep.2016.05.057

Gerfen, C. R., & Bolam, J. P. (2010). The neuroanatomical organization of the basal ganglia. In H. Steiner & K. Y. Tseng (Eds.), *Handbook of behavioral neuroscience* (Vol. 20, pp. 3–28). Elsevier, London.

Grealish, S., Diguet, E., Kirkeby, A., Mattsson, B., Heuer, A., Bramoulle, Y., … Parmar, M. (2014). Human ESC-derived dopamine neurons show similar preclinical efficacy and potency to fetal neurons when grafted in a rat model of Parkinson's disease. *Cell Stem Cell*, *15*(5), 653–665. https://doi.org/10.1016/j.stem.2014.09.017

Grealish, S., Heuer, A., Cardoso, T., Kirkeby, A., Jonsson, M., Johansson, J., … Parmar, M. (2015). Monosynaptic tracing using modified rabies virus reveals early and extensive circuit integration of human embryonic stem cell-derived neurons. *Stem Cell Reports*, *4*(6), 975–983. https://doi.org/10.1016/j.stemcr.2015.04.011

Grealish, S., Jonsson, M. E., Li, M., Kirik, D., Bjorklund, A., & Thompson, L. H. (2010). The A9 dopamine neuron component in grafts of ventral mesencephalon is an important determinant for recovery of motor function in a rat model of Parkinson's disease. *Brain*, *133*(Pt 2), 482–495. https://doi.org/10.1093/brain/awp328

Isacson, O., Deacon, T. W., Pakzaban, P., Galpern, W. R., Dinsmore, J., & Burns, L. H. (1995). Transplanted xenogeneic neural cells in neurodegenerative disease models exhibit remarkable axonal target specificity and distinct growth patterns of glial and axonal fibres. *Nature Medicine*, *1*(11), 1189–1194.

Kefalopoulou, Z., Politis, M., Piccini, P., Mencacci, N., Bhatia, K., Jahanshahi, M., … Foltynie, T. (2014). Long-term clinical outcome of fetal cell transplantation for Parkinson disease: Two case reports. *JAMA Neurology*, *71*(1), 83–87. https://doi.org/10.1001/jamaneurol.2013.4749

Kikuchi, T., Morizane, A., Doi, D., Magotani, H., Onoe, H., Hayashi, T., … Takahashi, J. (2017). Human iPS cell-derived dopaminergic neurons function in a primate Parkinson's disease model. *Nature*, *548*(7669), 592–596. https://doi.org/10.1038/nature23664

Kirkeby, A., Grealish, S., Wolf, D. A., Nelander, J., Wood, J., Lundblad, M., … Parmar, M. (2012). Generation of regionally specified neural progenitors and functional neurons from human embryonic stem cells under defined conditions. *Cell Reports*, *1*(6), 703–714. https://doi.org/10.1016/j.celrep.2012.04.009

Kordower, J. H., Freeman, T. B., Snow, B. J., Vingerhoets, F. J., Mufson, E. J., Sanberg, P. R., et al. (1995). Neuropathological evidence of graft survival and striatal reinnervation after the transplantation of fetal mesencephalic tissue in a patient with Parkinson's disease. *The New England Journal of Medicine*, *332*(17), 1118–1124. https://doi.org/10.1056/NEJM199504273321702

Kriks, S., Shim, J. W., Piao, J., Ganat, Y. M., Wakeman, D. R., Xie, Z., … Studer, L. (2011). Dopamine neurons derived from human ES cells efficiently engraft in animal models of Parkinson's disease. *Nature*, *480*(7378), 547–551. https://doi.org/10.1038/nature10648

Lelos, M. J., Morgan, R. J., Kelly, C. M., Torres, E. M., Rosser, A. E., & Dunnett, S. B. (2016). Amelioration of non-motor dysfunctions after transplantation of human dopamine neurons in a model of Parkinson's disease. *Experimental Neurology*, *278*, 54–61. https://doi.org/10.1016/j.expneurol.2016.02.003

Lerner, T. N., Shilyansky, C., Davidson, T. J., Evans, K. E., Beier, K. T., Zalocusky, K. A., … Deisseroth, K. (2015). Intact-brain analyses reveal distinct information carried by SNc dopamine subcircuits. *Cell*, *162*(3), 635–647. https://doi.org/10.1016/j.cell.2015.07.014

Li, W., Englund, E., Widner, H., Mattsson, B., van Westen, D., Latt, J., … Li, J. Y. (2016). Extensive graft-derived dopaminergic innervation is maintained 24 years after transplantation in the degenerating parkinsonian brain. *Proceedings of the National Academy of Sciences of the United States of America*, *113*(23), 6544–6549. https://doi.org/10.1073/pnas.1605245113

Lindvall, O., Brundin, P., Widner, H., Rehncrona, S., Gustavii, B., Frackowiak, R., et al. (1990). Grafts of fetal dopamine neurons survive

and improve motor function in Parkinson's disease. *Science*, *247*(4942), 574–577.

Menegas, W., Bergan, J. F., Ogawa, S. K., Isogai, Y., Umadevi Venkataraju, K., Osten, P., … Watabe-Uchida, M. (2015). Dopamine neurons projecting to the posterior striatum form an anatomically distinct subclass. *Elife*, *4*, e10032. https://doi.org/10.7554/eLife.10032

Morizane, A., Kikuchi, T., Hayashi, T., Mizuma, H., Takara, S., Doi, H., … Takahashi, J. (2017). MHC matching improves engraftment of iPSC-derived neurons in non-human primates. *Nature Communications*, *8*(1), 385. https://doi.org/10.1038/s41467-017-00926-5

Nolbrant, S., Heuer, A., Parmar, M., & Kirkeby, A. (2017). Generation of high-purity human ventral midbrain dopaminergic progenitors for in vitro maturation and intracerebral transplantation. *Nature Protocols*, *12*(9), 1962–1979. https://doi.org/10.1038/nprot.2017.078

Paxinos, G., & Watson, C. (2005). *The rat brain in stereotaxic coordinates* (5th ed.). London, UK: Academic Press.

Politis, M., Wu, K., Loane, C., Quinn, N. P., Brooks, D. J., Rehncrona, S., … Piccini, P. (2010). Serotonergic neurons mediate dyskinesia side effects in Parkinson's patients with neural transplants. *Science Translational Medicine*, *2*(38), 38ra46. https://doi.org/10.1126/scitranslmed.3000976

Rath, A., Klein, A., Papazoglou, A., Pruszak, J., Garcia, J., Krause, M., … Nikkhah, G. (2013). Survival and functional restoration of human fetal ventral mesencephalon following transplantation in a rat model of Parkinson's disease. *Cell Transplantation*, *22*(7), 1281–1293. https://doi.org/10.3727/096368912X654984

Smith, J. B., Klug, J. R., Ross, D. L., Howard, C. D., Hollon, N. G., Ko, V. I., … Jin, X. (2016). Genetic-based dissection unveils the inputs and outputs of striatal patch and matrix compartments. *Neuron*, *91*(5), 1069–1084. https://doi.org/10.1016/j.neuron.2016.07.046

Steinbeck, J. A., Choi, S. J., Mrejeru, A., Ganat, Y., Deisseroth, K., Sulzer, D., … Studer, L. (2015). Optogenetics enables functional analysis of human embryonic stem cell-derived grafts in a Parkinson's disease model. *Nature Biotechnology*, *33*(2), 204–209. https://doi.org/10.1038/nbt.3124

Steinbeck, J. A., & Studer, L. (2015). Moving stem cells to the clinic: Potential and limitations for brain repair. *Neuron*, *86*(1), 187–206. https://doi.org/10.1016/j.neuron.2015.03.002

Thompson, L. H., Grealish, S., Kirik, D., & Bjorklund, A. (2009). Reconstruction of the nigrostriatal dopamine pathway in the adult mouse brain. *The European Journal of Neuroscience*, *30*(4), 625–638. https://doi.org/10.1111/j.1460-9568.2009.06878.x

Wakeman, D. R., Hiller, B. M., Marmion, D. J., McMahon, C. W., Corbett, G. T., Mangan, K. P., … Kordower, J. H. (2017). Cryopreservation maintains functionality of human iPSC dopamine neurons and rescues parkinsonian phenotypes in vivo. *Stem Cell Reports*, *9*(1), 149–161. https://doi.org/10.1016/j.stemcr.2017.04.033

Watabe-Uchida, M., Zhu, L., Ogawa, S. K., Vamanrao, A., & Uchida, N. (2012). Whole-brain mapping of direct inputs to midbrain dopamine neurons. *Neuron*, *74*(5), 858–873. https://doi.org/10.1016/j.neuron.2012.03.017

Wickersham, I. R., Lyon, D. C., Barnard, R. J., Mori, T., Finke, S., Conzelmann, K. K., … Callaway, E. M. (2007). Monosynaptic restriction of transsynaptic tracing from single, genetically targeted neurons. *Neuron*, *53*(5), 639–647. https://doi.org/10.1016/j.neuron.2007.01.033

Wictorin, K., Brundin, P., Sauer, H., Lindvall, O., & Bjorklund, A. (1992). Long distance directed axonal growth from human dopaminergic mesencephalic neuroblasts implanted along the nigrostriatal pathway in 6-hydroxydopamine lesioned adult rats. *The Journal of Comparative Neurology*, *323*(4), 475–494. https://doi.org/10.1002/cne.903230403

Zufferey, R., Nagy, D., Mandel, R. J., Naldini, L., & Trono, D. (1997). Multiply attenuated lentiviral vector achieves efficient gene delivery in vivo. *Nature Biotechnology*, *15*(9), 871–875. https://doi.org/10.1038/nbt0997-871

How to cite this article: Cardoso T, Adler AF, Mattsson B, et al. Target-specific forebrain projections and appropriate synaptic inputs of hESC-derived dopamine neurons grafted to the midbrain of parkinsonian rats. *J Comp Neurol*. 2018;1–14. https://doi.org/10.1002/cne.24500